Effects of the ICRH resonance position on the profile shape of the W density in JET-ILW H-mode discharges

M. Sertoli[1,2], F. J. Casson [2], R. Bilato[1], I. Voitsekhovitch[2], J. Boom[1], E. Delabie[3], J. Flanagan[2], A. Shaw[2] and JET Contributors*

[1] *Max-Planck-Institut für Plasmaphysik, D-85748 Garching, Germany*,
[2] *CCFE, Culham Science Centre, Abingdon, Oxon, OX14 3DB, UK*,
[3] *Oak Ridge National Laboratory, Oak Ridge, TN 37830, USA*,
* *See the author list of X. Litaudon et al., Nucl. Fusion 57, 102001 (2017)*

The large mass tungsten (W) and its highly ionised states present in fusion-grade plasmas make it susceptible to centrifugal and electrostatic forces which lead to poloidal variations of its density within a flux-surface (see e.g. [1] and references therein). The theory describing the effects of this non-uniform poloidal distribution on the neoclassical transport of impurities has been found to be quite robust against experimental results (see e.g. [3] and references therein), but the inclusion of the effects of ion-cyclotron-resonance heating (ICRH) has proven to be more challenging. This is due to the difficulty in calculating the temperature anisotropy of the minority heated ions [2], especially when the ICRH resonance is located on the low-field-side (LFS), which can then impact the estimation of its effects on the high-Z impurity transport coefficients [3]. Both in present machines such as JET-ILW, where ICRH deposited close to the plasma centre is often necessary to avoid tungsten (W) accumulation, and in future ones such as ITER, where the ICRH systems are planned to account for almost a third of total heating power, the optimisation of ICRH for impurity control can lead to longer, more stable plasma operation as well as free other systems such as electron-cyclotron-resonance-heating (ECRH) for other purposes such as neoclassical tearing mode (NTM) control and current profile tailoring.

In this contribution JET-ILW H-mode discharge 85377 has been studied ($I_P = 2.5\,MA$, $P_{NBI} = 15\,MW$ and $P_{ICRH} = 3.8\,MW$ in H-minority with $n_H/n_e \sim 6\%$ and $f = 42.5\,MHz$, dipole phas-

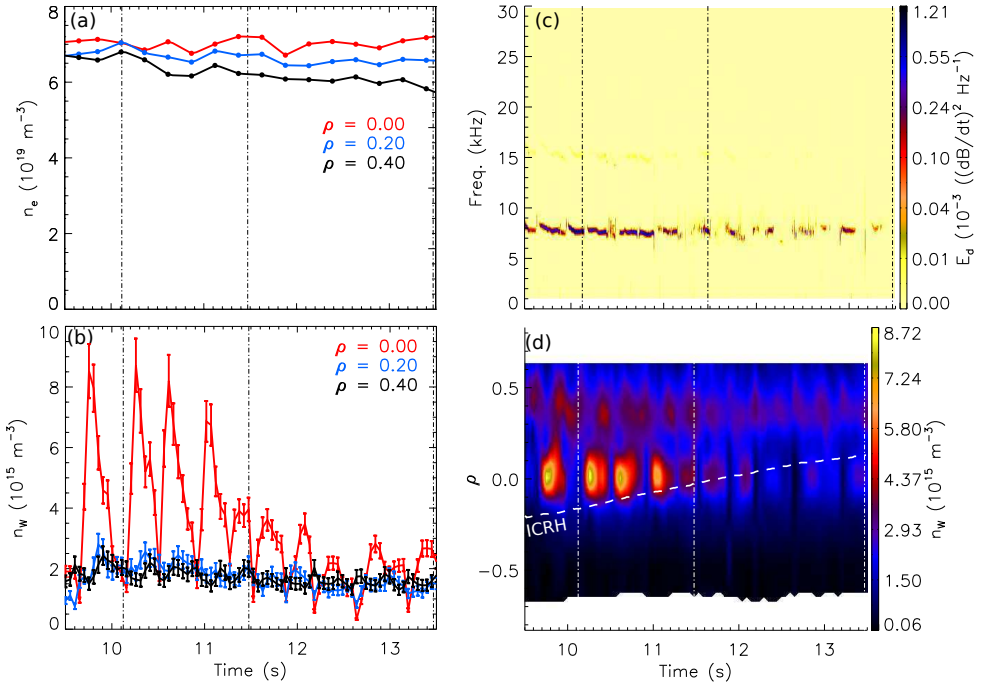

Figure 1: *JET pulse 85377, time evolution of: (a) electron density from (LIDAR) at* $\rho_t = 0.0$, 0.2 *and* 0.4 *(red, blue and black respectively); (b) flux-surface averaged W density; (c) spectrogram of magnetic coil T001; (d) midplane W density (*$\rho > 0$ *correspond to LFS,* $\rho < 0$ *to HFS. Dashed horizontal line in (d) shows the position of the ICRH resonance; dashed vertical lines indicate the time-points whose profiles are plotted in figures 2 and 3.*

ing, $Z_{eff} \sim 1.15$) to investigate the effect of the ICRH resonance location on the shape of the intrinsic W density. During 3 s of the flat-top phase the toroidal magnetic field has been varied from $B_t = 2.5$ to 2.85 T, moving the ICRH resonance layer in range $R \sim R_{ax} \pm 15$ cm, corresponding to $\rho_t \sim 0.1$ on the high-field-side (HFS) and low-field-side (LFS) respectively. T he resonance remains always well inside the sawtooth inversion radius ($\rho_{inv} \sim 0.3$), thus avoiding fundamental modifications in impurity transport at the crossing of $q = 1$, such as standard sawtooth cycles (peaked pre-crash impurity density) giving way to inverted ones (hollow pre-crash impurity density). All sawtooth cycles in the time-range of interest are in fact inverted ones (typical for strong RF-heating inside the $q = 1$ surface). The sawtooth period is also very stable (figure 1b), but the strength and characteristics of the $m/n = 1/1$ magneto-hydro-dynamic (MHD) activity changes slightly, with saturated modes lasting almost the whole sawtooth period at the beginning of the scan giving way to shorter saturation periods and phases with fishbones (figure 1c). The frequency of these modes is nonetheless constant at ~ 7.5 kHz throughout the whole time-range of analysis, as do the toroidal rotation and ion temperature (figures 3b and 3c). The electron temperature and density are instead constantly evolving (figure 1a, 3a-b), their peaking increasing even after the ICRH resonance has crossed the magnetic axis (at ~ 11.5 s) and the ELM frequency also roughly doubles (from ~ 30 Hz to ~ 60 Hz) throughout the time-range of analysis. These changes in background conditions complicate the interpretation of the whole discharge, but not the analysis of the equilibrium W density just before the sawtooth crashes which can then be compared with modelling estimates.

Two-dimensional maps of the experimental intrinsic W density profile have been determined coupling data from the SXR diagnostic and vacuum-ultra-violet (VUV) spectroscopy using the method explained in [4] recently upgraded to account for poloidal asymmetries [5]. For the present analysis, the following diagnostics have been used: 35 channel vertical SXR camera V, VUV spectrometer $KT7/3$ (set to the ~ 5 nm wavelength region), LIDAR Thomson scattering for both electron density and temperature, charge-exchange-recombination-spectroscopy (CXRS) for ion temperature and toroidal rotation measurements. The re-mapping of all the quantities has been performed using the EFIT equilibrium reconstruction rigidly shifted of 2 cm to the high field side so to match a separatrix temperature of ~ 100 eV as measured by HRTS. On top of this, a 1% increase of the toroidal magnetic field (relevant for a correct positioning of the ICRH resonance layer) has also been estimated for mapping of the electron temperature from electron-cyclotron emission (ECE, not shown here), both at the separatrix as well matching LFS and HFS channels when crossing the magnetic axis. With these assumptions, the results

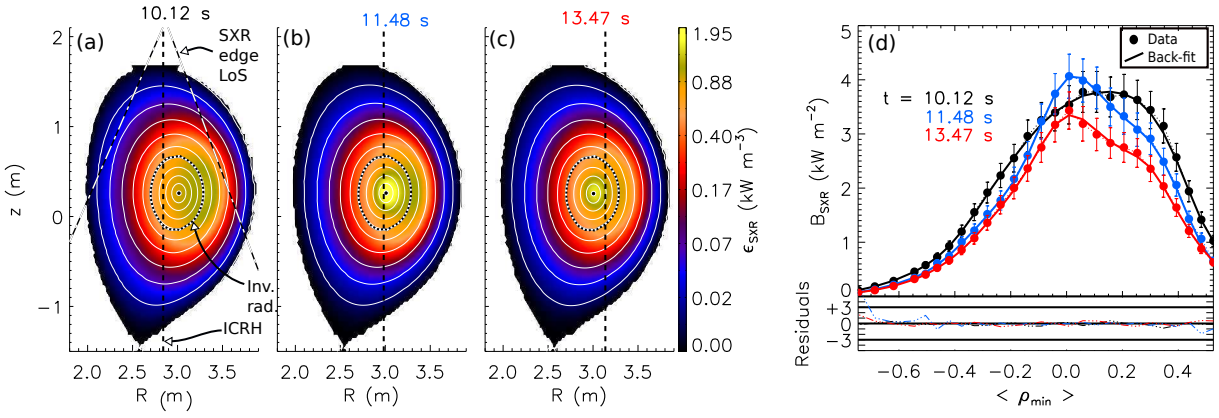

Figure 2: *(a,b,c) deconvoluted 2D SXR emissivity; (d) SXR brightness (dashed lines, points with error bars) compared with back-fitted LoS-integrals (continuous lines) at the three time-points (see label) indicated with dashed vertical lines in figure 1. Also shown and labelled in (a): SXR most edge LoS, ICRH resonance ρ_{ICRH} and inversion radius ρ_{inv}.*

obtained using the different electron profile diagnostics (HRTS , ECE or LIDAR Thomson scattering) are all within a few percent. Contributions from low-Z impurities and main ion (D) have been included using the visible Bremmstrahlung Z_{eff} measurement [6] with the assumption that their contributions are poloidally symmetric and that the only other impurity contaminating the plasma (apart from W) is Be.

The observed slow ($> \tau_{ST}$) decrease in flux-surface-averaged W density, whose peak central value drops of a factor $\sim 2-3$ over the time-range of interest (red in figure 1b) and the value at mid radius of ~ 30 % (black in figure 1b), is most probably due to increased ELM flushing caused by rising ELM frequency. Since the scope of this contribution is not to perform a source/sink balance, this will not be investigated further and the rest of the contribution will concentrate on the profile shape of the W density close to the end of the sawtooth cycles in three different phases with the ICRH resonance positioned at $R_{ax}-15\ cm$, R_{ax} and $R_{ax}+15\ cm$ (analysed time-points shown as vertical dashed lines in figures 1, the corresponding ICRH resonance position as vertical dashed lines in figures 2a-c and figures 3). For completeness, the 2D maps of the SXR emissivity resulting from the model-based deconvolution are shown in figure 2a-c, and the comparison of the SXR brightness with the back-fitted LoS-integrals (figure 2d) proves the quality of the reconstruction.

From the profile plots it is clear that, while the electron temperature peaks in the plasma centre and the values outside of the inversion radius remaining unaltered (figure 3b), the electron density peaking is a phenomena taking place across the whole profile, with the central value remaining constant (figure 3a). The resulting increase in normalised gradients $\rho = 0.1$ is $R/L_{Te} \sim 3 \rightarrow 4$ and $R/L_{ne} \sim 0 \rightarrow 1.5$. Within the experimental uncertainties, very similar results are obtained using HRTS in the place of LIDAR. With only one CXRS data-point inside $\rho < 0.4$ and the resulting high experimental uncertainties, the electron to ion temperature ratio in the centre stays constant at $T_e(0)/T_i(0) \sim 1.5$. In spite of these large uncertainties in the CXRS profiles, a confirmation of the toroidal rotation estimate is given by the frequency of the $1/1$ modes which fits well with the v_{rot} value close to the inversion radius (green diamond in figure 3c).

The profile shape of the flux-surface-averaged W density (figure 3d) roughly follows that of the electron density: hollow with flat electron density (black) and centrally peaked for peaked electron density (blue and red). The W density in-out asymmetry (figure 3e) matches well the theoretical estimates (continuous lines) assuming centrifugal effects (CF) only for $\rho_t > 0.3$. Inside this radius the experimental values show no detectable modifications due to the change in ICRH resonance location and are slightly lower than the CF-only limit. The asymmetry calculated including RF fast-particle contributions (minority fast temperature screening (FTS) and temperature anisotropy) calculated with TORIC-SSFPQL [2], leads to a slightly better match with experiment, but the difference is within the measurement error bars (dot-dashed line in figure 3h).

The W profile predicted using JETTO-SANCO-NEO [9, 10] using the measured bulk profiles and Bohm-GyroBohm transport for the turbulent diffusion, shows a very good match with experiment when the ICRH resonance is located on the HFS (black in figure 3g) already including CF-effects only. For the case of central and LFS resonance location, the CF-only model instead clearly overestimates the peaking. Including RF-effects from TORIC-SSFPQL, the match with experiment is still very good for the HFS case, while for central or LFS cases the impact of RF is clearly overestimated, with the modelled profiles resulting hollow inside $\rho_t < 0.2$ (consistent with what previously reported in [8]). Looking at the heat deposition profiles and integrated heating power (figure 3f and 3i), it is interesting to note that when the ICRH resonance is located on the LFS (red) the electron heating is highly enhanced with respect to the case with the resonance on the HFS. This is substantiated by the observed increase in electron temperature, but not fully in agreement with previous findings (e.g. [8]) where strong electron heating is

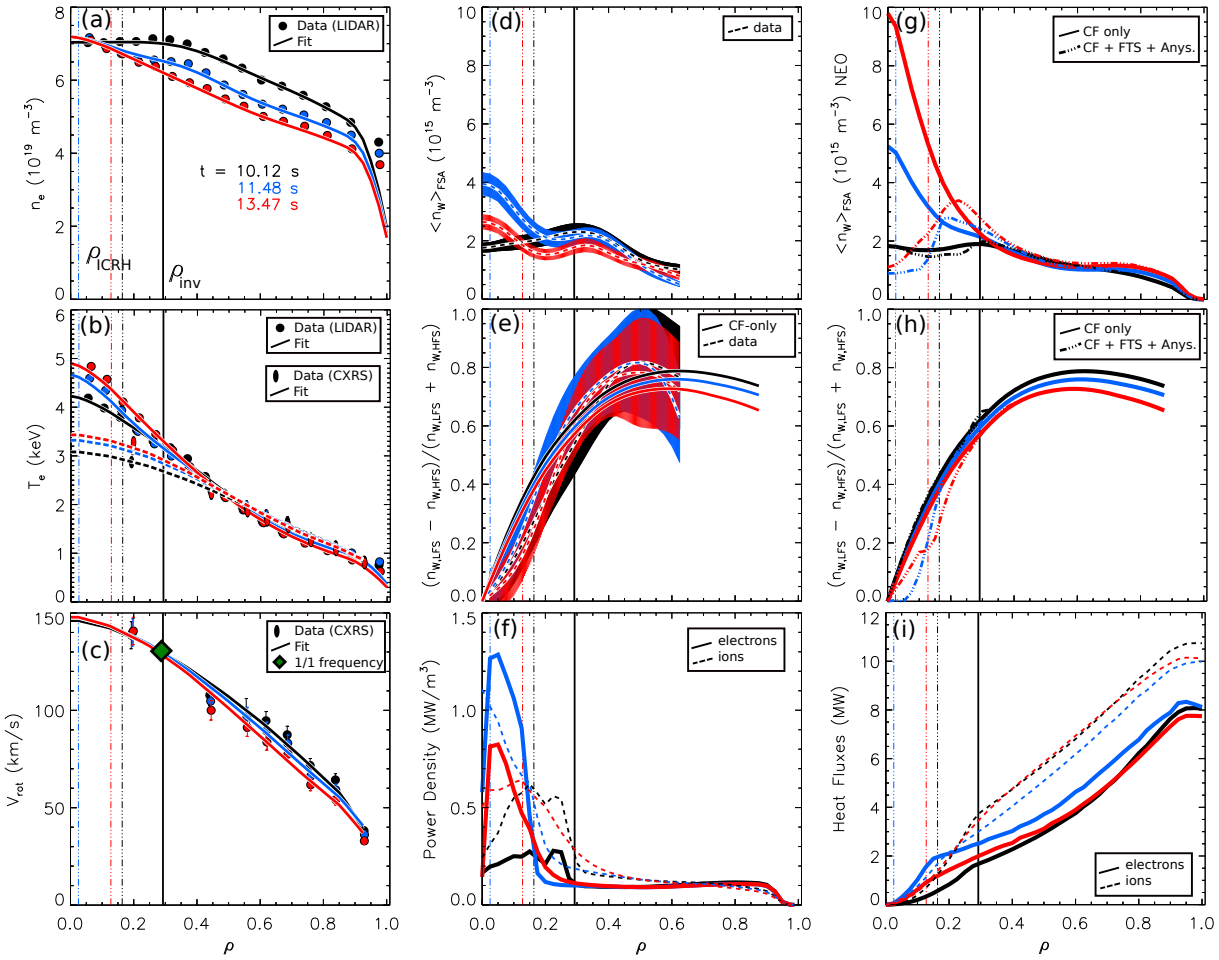

Figure 3: *Profiles for the time-points with ICRH resonance at $R_{ax} - 15$ cm (black), R_{ax} (blue), $R_{ax} + 15$ cm (red), time-points labelled in (a): (a) electron density; (b) electron and ion temperature; (c) toroidal rotation; (d) experimental flux-surface-averaged W density and (g) its modelling with CF-effects only compared to case including CF, FTS and RF-anisotropy; (e) experimental in-out asymmetry compared to CF-only model and (h) modelled in-out asymmetry including ICRH compared to CF-only model; (f) total (NBI + ICRH) power density and (i) integrated heating power to electrons and ions.*

typically associated with flattening of the electron density.

In conclusion, direct experimental identification of the RF anisotropy effect on asymmetry of W is difficult at JET, but can be inferred from W transport modelling. For the analysed discharge, the shape of the intrinsic W density is relatively well captured by neoclassical modelling if the ICRH resonance is located on the HFS and the impact of RF-effects is negligible. For the case with central and LFS resonance location, RF effects on transport are likely to be overstimated, but centrifugal effects alone are also not sufficient, predicting much more peaked profiles than experimentally observed. More investigations are needed to assess not only the sensitivity of the experimental results to the input parameters (e.g. equilibrium reconstruction), but as well the impact of approximations in the modelling such as the absence finite-orbit-width effects.

Acknowledgments: This work has been carried out within the framework of the EUROfusion Consortium and has received funding from the Euratom research and training programme 2014-2018 under grant agreement No 633053. The views and opinions expressed herein do not necessarily reflect those of the European Commission.

References: [1] T Odstrcil et al 2018 Plasma Physics and Controlled Fusion 60, 014003. [2] R Bilato et al 2017 Nucl. Fusion 57 056020. [3] F J Casson et al 2015 Plasma Phys. Control. Fusion 57 014031. [4] M Sertoli et al 2015 Plasma Phys. Controlled Fusion 57, 075004. [5] M Sertoli 2018 Submitted to Review of Scientific Instruments. [6] K H Behringer et al 1986 Nucl. Fusion 26, 751. [7] J Wesson et al 1997 Nucl. Fusion 37, 577. [8] C Angioni et al 2017 Nucl. Fusion 57 056015 [9] E A Belli et al 2012 Plasma Phys. Controlled Fusion 54, 015015 [10] S Breton et al accepted in Nucl. Fusion doi.org/10.1088/1741-4326/aac780